Available online at www.sciencedirect.com
SCIENCE DIRECT®
Acta Materialia 53 (2005) 4189–4197
Acta MATERIALIA
www.actamat-journals.com

Application of the cluster/site approximation to fcc phases in Ni–Al–Cr system

W. Cao [a], J. Zhu [a], Y. Yang [a], F. Zhang [b], S. Chen [b], W.A. Oates [c], Y.A. Chang [a,*]

[a] *Department of Materials Science and Engineering, University of Wisconsin, 1509 University Avenue, Madison, WI 53706 1595, USA*
[b] *CompuTherm LLC, 437 South Yellowstone Drive, Madison, WI 53719, USA*
[c] *Institute for Materials Research, University of Salford, Salford M5 4WT, UK*

Received 9 February 2005; received in revised form 4 May 2005; accepted 11 May 2005
Available online 1 July 2005

Abstract

The cluster/site approximation (CSA) has been used to model the face-centered cubic (fcc) phases (disordered γ with A1 structure and ordered γ' with $L1_2$ structure) in the Ni–Al–Cr ternary system. The CSA takes into account short-range order (SRO), which is essential to satisfactorily describe the thermodynamics of order/disorder transitions such as occur between the fcc phases in the Ni–Al–Cr system. It possesses computational advantages over the cluster variation method (CVM) while offering comparable accuracy in the calculation of multi-component phase diagrams. This makes the CSA a practical method for carrying out calculations on real alloy systems. These points are illustrated in the application of the CSA to fcc phases in the Ni–Al–Cr system. The CSA-calculated phase diagrams, which use fewer model parameters than used in previous descriptions, based on the point approximation, are in good accord with the experimental data. In addition, the fcc metastable phase diagrams calculated by using the CSA show reasonable ordering/disordering behavior and phase relationships.

Keywords: Nickel alloys; Cluster/site approximation; Cluster variation method; Order–disorder phenomena; Phase diagram

1. Introduction

The Ni–Al–Cr ternary system has been studied extensively due to the importance of these three elements in Ni-based superalloys. The latter consist mainly of two phases: γ with the A1 structure and γ' with the $L1_2$ structure being an ordered state of the face-centered cubic (fcc) (A1) lattice. In addition to the large amount of experimental measurements on phase equilibria and thermodynamics, several thermodynamic descriptions for this system, based on the CALPHAD method, have been published.

A recent thermodynamic description by Huang and Chang [1] was quite successful in describing the experimental data. This description gives a better account, with fewer model parameters than an earlier one given by Dupin [2]. However, in the Huang and Chang's description, the two fcc phases, γ and γ', were modeled separately. The disordered γ phase was modeled with a substitutional solution model, while a two sublattice compound energy model [3] was used for the ordered γ' phase. Later, Dupin et al. [4] modeled both phases by a Gibbs energy function which is a sum of two contributions, one corresponding to the Gibbs energy of the disordered phase and the other to the ordering Gibbs energy. In all these descriptions [1,2,4], the γ and γ' phases have been described using models based on the point or Bragg–Williams approximation. This type of approximation is known to give problems with

* Corresponding author. Tel.: +1 608 262 0389; fax: +1 608 262 8353.
E-mail address: chang@engr.wisc.edu (Y.A. Chang).

1359-6454/$30.00
doi:10.1016/j.actamat.2005.05.016

phase diagram topology, particularly for fcc-based systems, basically because it cannot take into account the existence of short-range order (SRO) [5–7]. Accordingly, these descriptions are often not reliable in extrapolating the thermodynamic properties to metastable regions or in extrapolating the thermodynamic descriptions of the lower order systems to the multi-component systems.

The cluster variation method (CVM) [8] is superior to the point approximation in that it takes SRO into consideration. Good agreement for fcc prototype systems with the results from Monte-Carlo simulation based on the same energy parameters can be obtained by using the CVM. A major disadvantage of the CVM, however, is that it is computationally too intensive for use with multi-component systems. This stems from the fact that the independent variables in the CVM are essentially the cluster probabilities, of which there are C^n, where C is the number of components and n the number of atoms in the cluster. As a result, an extremely large number of non-linear equations must be solved simultaneously when multi-component alloys are considered.

On the other hand, the cluster/site approximation (CSA) [9,10] also considers the existence of SRO but is computationally much less demanding because the independent variables are essentially the point probabilities. Since there are only $C \times n$ point probabilities as compared with C^n cluster probabilities, the computational advantage of the CSA is obvious. The CSA has been used successfully in the calculation of the prototype ternary system Cu–Ag–Au [11], where it was shown that, in spite of the considerably reduced computational effort, the CSA could achieve comparable accuracy with the CVM in the tetrahedron approximation for multi-component systems. This prototype study confirmed the CSA as a practical possibility for calculations on real multi-component alloy systems.

Recently, the fcc phases in the Ni–Al binary system have been modeled using the CSA [12] and the calculated phase diagram topology for metastable fcc phases is comparable with that obtained from a "first principle" + CVM calculation [13,14], which, as will be discussed later, is not the case for the previous descriptions based on the point approximation [1,2,4]. In this spirit, we have explored the possibility of applying the CSA to the fcc phases in the Ni–Al–Cr ternary system while retaining the earlier descriptions of the other phases [1,12]. The new description may be used not only for calculating the stable phase diagram but also for calculating the metastable phase diagrams.

2. The cluster/site approximation

The formalism used in the CSA was introduced many years ago by Fowler [15] for treating atom/molecule equilibria in gases and subsequently used for clusters in solid solutions by Yang and Li [16–19], where it can be used to describe both long-range order (LRO) and SRO. In the CSA the clusters must be energetically non-interfering, thus, they are permitted to share only corners and not faces or edges. In this case, there are only two terms in the entropy expression, the cluster entropy and the single-site entropy. The entropy per site S_m can be written as

$$S_m = \zeta S_n - (n\zeta - 1)S_1, \tag{1}$$

where ζ is the number of energetically non-interfering clusters per site. In the nearest-neighbor pairwise approximation, as was used by Yang and Li, $\zeta = z/2p$, z being the nearest-neighbor coordination number and p the number of nearest-neighbor pairs in the cluster of size n. The dimensionless cluster and site entropies S_n, S_1 are given by $S_n = -\sum_i Z_i \ln Z_i$ and $S_1 = -\sum_i X_i \ln X_i$, respectively, where Z_i is the cluster probability, X_i the site probability.

In the CSA, the molar equilibrium free energy F_m for system with C components is given by [10]

$$\frac{F_{\mathrm{m}}}{RT} = \zeta\left(\sum_{P}^{C-1}\sum_{i=1}^{n} y_P^i \mu_P^i - \ln\lambda\right) - (n\zeta - 1)\left(\sum_{P}^{C}\sum_{i=1}^{n} f_i y_P^i \ln y_P^i\right), \tag{2}$$

where f_i is the fraction of sublattice of type i, y_P^i is the sublattice mole fraction of component P on sublattice i. The μ_P^i are Lagrangian multipliers arising from the mass balance constraints and are related to the species chemical potentials of the atoms on the sublattice i. The cluster partition function, λ, is expressed in terms of the cluster energies and the μ_P^i.

The coherent fcc phase diagram calculated from the original Yang–Li formulism represented by the above equations with $\zeta = z/2p$ is at variance with that obtained from MC simulations [20] and CVM calculations [21]. Although the separation of the three critical regions for the $L1_0$ and the two $L1_2$ phases is correctly found, the disordered A1 phase is incorrectly predicted to be stable down to zero Kelvin at compositions between the ordered $L1_2$ and $L1_0$ phases. By permitting ζ to deviate by a small amount from the value given by $(z/2p)$, it is possible to overcome the problems of the original Yang–Li formulation [10]. Good agreement with the binary alloy fcc prototype phase diagrams derived from either MC simulations or from using the CVM in the tetrahedron approximation can be achieved [21] by using ζ as an adjustable parameter.

The application of the CSA to real alloy systems also requires taking into account of both atomic size mismatch and excitational contributions in the expression

for the free energy of mixing. The excitational contributions are coarse-grained into the configurational free energy which, in the high temperature approximation, leads to a linear temperature variation of the cluster energies. For the atomic size mismatch, the method suggested by Ferreira et al. [22] is used in which the elastic energy is assumed configuration independent (volume changes between ordered and disordered phases are very small) so that the expression for the free energy becomes

$$F_{\mathrm{m}} = F_{\mathrm{CD}} + F_{\mathrm{CI}}, \tag{3}$$

where F_{CD} are the configuration-dependent and F_{CI} the configuration-independent contributions, respectively. The first term, F_{CD}, is determined by Eq. (2) while the second term in Eq. (3), F_{CI}, can be expressed as a Redlich–Kister polynomial of the mole fractions x and temperature T, with coefficients L

$$F_{\mathrm{CI}} = \sum_{P,Q} x_P x_Q (L_0 + L_1(x_P - x_Q) + \cdots) \tag{4}$$

in which P, Q are components.

Eq. (3) is then seen to be a function of the temperature-dependent cluster energies, the geometrical factor ζ, the temperature T, the Lagrangian multipliers μ_P^i and the coefficients L. Both the ζ and L parameters and the temperature-dependent cluster energies are used as optimizing parameters to obtain a satisfactory description of the experimental data.

With these modifications to the original CSA, it is possible to obtain good descriptions for the free energies of mixing for real alloy systems [10,14,23,24].

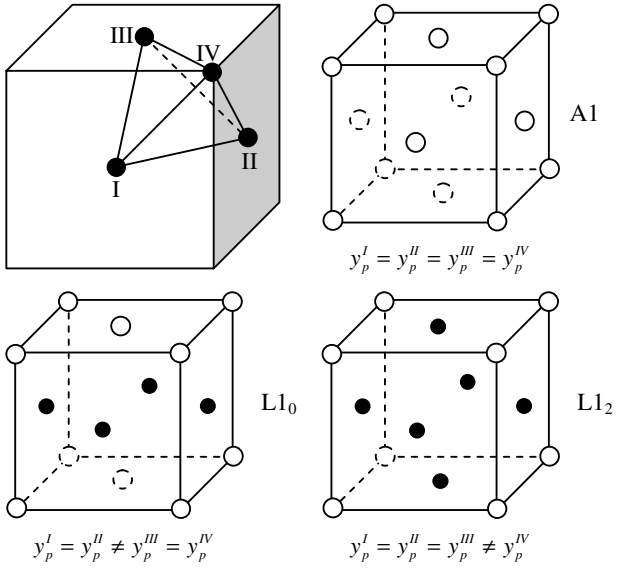

Fig. 1. A tetrahedron cluster taken from face-centered cubic lattice containing four sites and the corresponding phases represented by the model.

3. Application of the CSA to the Ni–Al–Cr system

In the Ni–Al–Cr system, there are three principle phases: liquid (L), fcc, body-centered cubic, where the fcc phase has two different stable states, i.e., the disordered state (A1), represented by γ in the stable phase diagram, and the ordered state ($L1_2$), represented by γ'. Since the objective of this study was to explore the possibility of the application of the CSA to the real Ni–Al–Cr alloys, only the fcc phase has been modeled using the CSA.

To represent the fcc phases, the nearest-neighbor tetrahedron cluster shown in Fig. 1 was chosen. Using this cluster, there are four sublattices and the phase may be represented by $(\mathrm{Ni, Al, Cr})_{0.25}$:$(\mathrm{Ni, Al, Cr})_{0.25}$:$(\mathrm{Ni, Al, Cr})_{0.25}$:$(\mathrm{Ni, Al, Cr})_{0.25}$. The corresponding sublattice mole fractions or the site occupation fractions for Ni, Al and Cr on each sublattice are y_{Ni}^i, y_{Al}^i and y_{Cr}^i (i = I, II, III and IV). When the fcc phase is in the disordered A1 state, we have $y_P^{\mathrm{I}} = y_P^{\mathrm{II}} = y_P^{\mathrm{III}} = y_P^{\mathrm{IV}} = x_P$, whereas $y_P^{\mathrm{I}} = y_P^{\mathrm{II}} \neq y_P^{\mathrm{III}} = y_P^{\mathrm{IV}}$ for $L1_0$ and $y_P^{\mathrm{I}} = y_P^{\mathrm{II}} = y_P^{\mathrm{III}} \neq y_P^{\mathrm{IV}}$ for the $L1_2$ structure, P being any of the component of Ni, Al or Cr. Accordingly, there is a total of 81 different possible tetrahedron clusters in the Ni–Al–Cr ternary system. The number of corresponding cluster energies can be considerably reduced by assuming that the energies depend on the composition but not on the arrangements of the cluster atoms. This is conveniently done by relating the cluster energies to the nearest-neighbor pairwise energies ω_{ij}. These are then optimized together with the geometrical factor ζ and the L parameters in F_{CI}, Eq. (4).

4. Results and discussion

Optimization of model parameters and the subsequent phase diagram calculations were carried out using Pandat [25]. Since the fcc phase in the Ni–Al binary has already been modeled using the CSA by Zhang et al. [12], their description was used in the present study. The model parameters for the fcc phase in the other two binaries and in the ternary were optimized in terms of the experimental data assessed by Huang and Chang [1]. The model parameters for the fcc phase obtained from optimization are listed in Table 1.

In order to permit a comparison between the calculated results and the available experimental data in [1], three isothermal sections were calculated at 1273, 1423 and 1473 K. In the CSA-calculated isothermal section at 1273 K, shown in Fig. 2, the γ' single-phase region is slightly more extensive as compared with that given by Taylor and Floyd [26], while it agrees very well with the experimental data of Ochiai et al. [27], shown in Fig. 3. A similar conclusion was reached concerning these results in Huang's description [1]. It should be pointed out that the $\gamma/\gamma + \gamma'$ phase boundary calculated in the present

Table 1
Model parameters for fcc phase of the Ni–Al–Cr system developed by present study

Ni–Al binary (from [12])	$\omega_{\mathrm{AlNi}} = -16{,}615 + 1.6333 \cdot T$
	$\varepsilon_{\mathrm{AlNi_3}} = 0.25 \cdot G^{\mathrm{fcc}}_{\mathrm{Al}} + 0.75 \cdot G^{\mathrm{fcc}}_{\mathrm{Ni}} + 3 \cdot \omega_{\mathrm{AlNi}}$
	$\varepsilon_{\mathrm{Al_2Ni_2}} = 0.5 \cdot G^{\mathrm{fcc}}_{\mathrm{Al}} + 0.5 \cdot G^{\mathrm{fcc}}_{\mathrm{Ni}} + 4 \cdot \omega_{\mathrm{AlNi}}$
	$\varepsilon_{\mathrm{Al_3Ni}} = 0.75 \cdot G^{\mathrm{fcc}}_{\mathrm{Al}} + 0.25 \cdot G^{\mathrm{fcc}}_{\mathrm{Ni}} - 20{,}000$
	${}^0L = 13{,}500 + 10 \cdot T$
	${}^1L = -24{,}460 + 7.484 \cdot T$
	${}^2L = 6600 - 4 \cdot T$
Al–Cr binary	$\omega_{\mathrm{AlCr}} = -1250$
	$\varepsilon_{\mathrm{AlCr_3}} = 0.25 \cdot G^{\mathrm{fcc}}_{\mathrm{Al}} + 0.75 \cdot G^{\mathrm{fcc}}_{\mathrm{Cr}} + 3 \cdot \omega_{\mathrm{AiCr}}$
	$\varepsilon_{\mathrm{Al_2Cr_2}} = 0.5 \cdot G^{\mathrm{fcc}}_{\mathrm{Al}} + 0.5 \cdot G^{\mathrm{fcc}}_{\mathrm{Cr}} + 4 \cdot \omega_{\mathrm{AlCr}}$
	$\varepsilon_{\mathrm{Al_3Cr}} = 0.75 \cdot G^{\mathrm{fcc}}_{\mathrm{Al}} + 0.25 \cdot G^{\mathrm{fcc}}_{\mathrm{Cr}} + 3 \cdot \omega_{\mathrm{AiCr}}$
	${}^0L = -30{,}203.8 + 5.67993 \cdot T$
Cr–Ni binary	$\omega_{\mathrm{CrNi}} = -3831$
	$\varepsilon_{\mathrm{CrNi_3}} = 0.25 \cdot G^{\mathrm{fcc}}_{\mathrm{Cr}} + 0.75 \cdot G^{\mathrm{fcc}}_{\mathrm{Ni}} + 3 \cdot \omega_{\mathrm{CrNi}}$
	$\varepsilon_{\mathrm{Cr_2Ni_2}} = 0.5 \cdot G^{\mathrm{fcc}}_{\mathrm{Cr}} + 0.5 \cdot G^{\mathrm{fcc}}_{\mathrm{Ni}} + 4 \cdot \omega_{\mathrm{CrNi}}$
	$\varepsilon_{\mathrm{Cr_3Ni}} = 0.75 \cdot G^{\mathrm{fcc}}_{\mathrm{Cr}} + 0.25 \cdot G^{\mathrm{fcc}}_{\mathrm{Ni}} + 3 \cdot \omega_{\mathrm{CrNi}}$
	${}^0L = 59{,}735 - 15.1119 \cdot T$
	${}^1L = 37{,}521.8 - 18.8876 \cdot T$
Ni–Al–Cr ternary	$\zeta = 1.35$
	$\varepsilon_{\mathrm{Al_2CrNi}} = 0.5 \cdot G^{\mathrm{fcc}}_{\mathrm{Al}} + 0.25 \cdot G^{\mathrm{fcc}}_{\mathrm{Cr}} + 0.25 \cdot G^{\mathrm{fcc}}_{\mathrm{Ni}} + 2 \cdot \omega_{\mathrm{AlCr}} + 2 \cdot \omega_{\mathrm{AlNi}} + \omega_{\mathrm{CrNi}} - 1900$
	$\varepsilon_{\mathrm{AlCr_2Ni}} = 0.25 \cdot G^{\mathrm{fcc}}_{\mathrm{Al}} + 0.5 \cdot G^{\mathrm{fcc}}_{\mathrm{Cr}} + 0.25 \cdot G^{\mathrm{fcc}}_{\mathrm{Ni}} + 2 \cdot \omega_{\mathrm{AlCr}} + \omega_{\mathrm{AlNi}} + 2 \cdot \omega_{\mathrm{CrNi}} - 1900$
	$\varepsilon_{\mathrm{AlCrNi_2}} = 0.25 \cdot G^{\mathrm{fcc}}_{\mathrm{Al}} + 0.25 \cdot G^{\mathrm{fcc}}_{\mathrm{Cr}} + 0.5 \cdot G^{\mathrm{fcc}}_{\mathrm{Ni}} + \omega_{\mathrm{AlCr}} + 2 \cdot \omega_{\mathrm{AlNi}} + 2 \cdot \omega_{\mathrm{CrNi}} + 6100$

study, when compared with the results in [1], gives a better account of the experiment data at this temperature. Further comparisons between the CSA-calculated results with the experimental data at 1423 [26] and 1473 K [28,29] are shown in Figs. 4 and 5, respectively. It can be seen that they are in reasonable accord with the experimental results.

The CSA-calculated γ solvus values are compared with those measured by Hong et al. [30] in Figs. 6 and 7, respectively. Fig. 6 shows a comparison of the

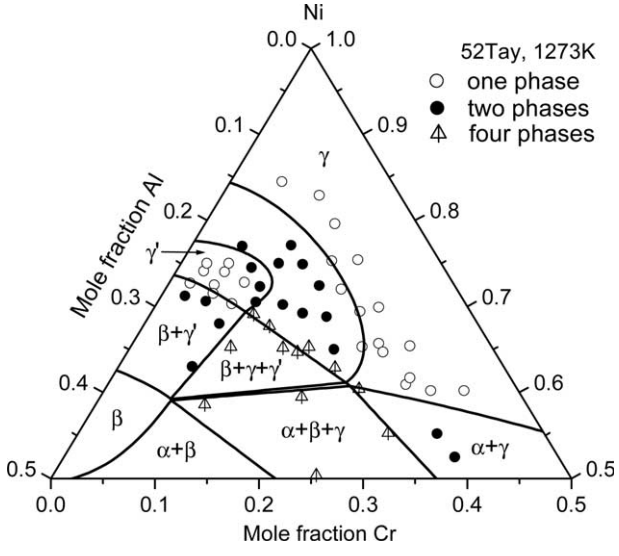

Fig. 2. Comparison of the CSA-calculated isothermal section at 1273 K with the experimental data. Note: according to Taylor and Floyd [26], 1273 K is the four-phase ($\gamma + \gamma' + \beta + \alpha$) equilibrium temperature.

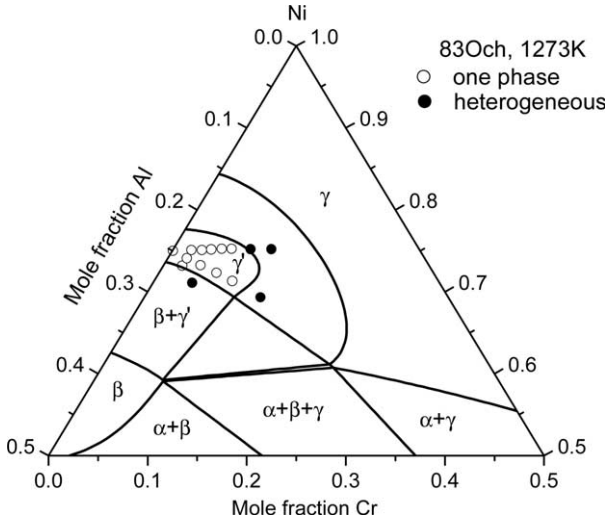

Fig. 3. Comparison of the CSA-calculated isothermal section at 1273 K with the experimental data.

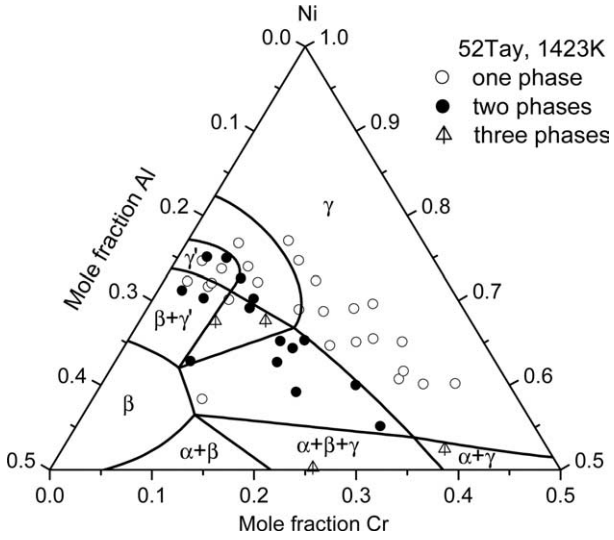

Fig. 4. Comparison of the CSA-calculated isothermal section at 1423 K with the experimental data.

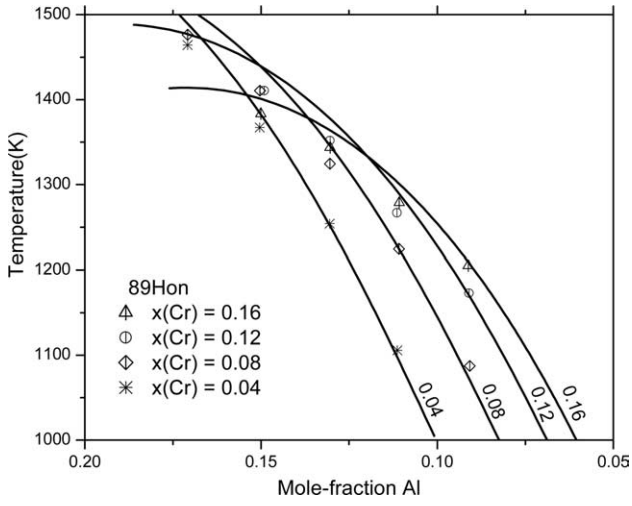

Fig. 6. Comparison of the CSA-calculated γ solvus of constant Cr concentrations with the experimental data.

calculated γ solvus with the experimental data, where each line or symbol represents a constant Cr content but with varying concentrations of Al. As can be seen, the calculated results are in good agreement with the experimental data. In Fig. 7, the concentrations of Al are kept constant while the Cr concentration is varied. Since some experimental data for high Cr contents, as pointed by Huang et al. [1], might be for metastable $\gamma/\gamma + \gamma'$ equilibria, the calculated results failed to fit them very well. For those points with lower Cr contents, however, the calculated results are in good agreement with the experimental data. We have also examined the liquidus projection and the isothermal sections involved with the fcc phase at other temperatures. All these results gave comparable accounts of the experimental data with those obtained from the Huang and Chang's descriptions. On the other hand, it should be pointed out that the number of parameters used to describe the thermodynamic properties of the fcc phase in the present study is 20, while it is 28 in the Huang and Chang description. Despite the considerably reduced number of the model parameters, the use of the CSA still permits good agreement with the experimental data.

As noted in the introduction, since the CSA has the advantage over the point approximation by taking the SRO into consideration, it is more suitable to describe the order/disorder transition. Zhang et al. [12] have demonstrated that the CSA-calculated fcc metastable phase diagram for the Ni–Al system is what one expects. In other words, the disordered A1 is stable at higher

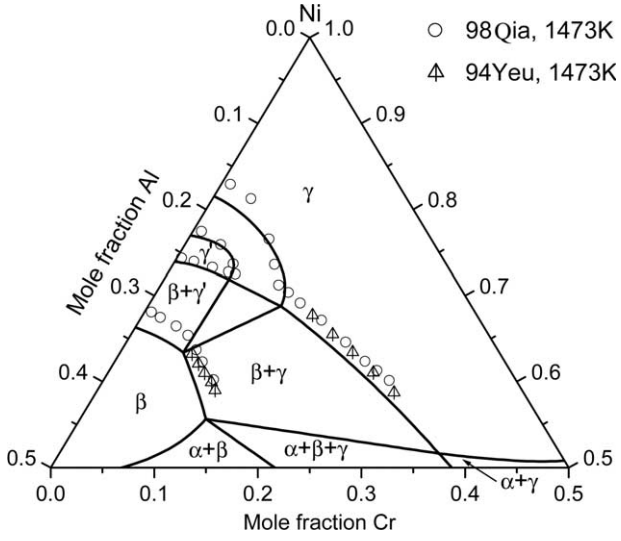

Fig. 5. Comparison of the CSA-calculated isothermal section at 1473 K with the experimental data.

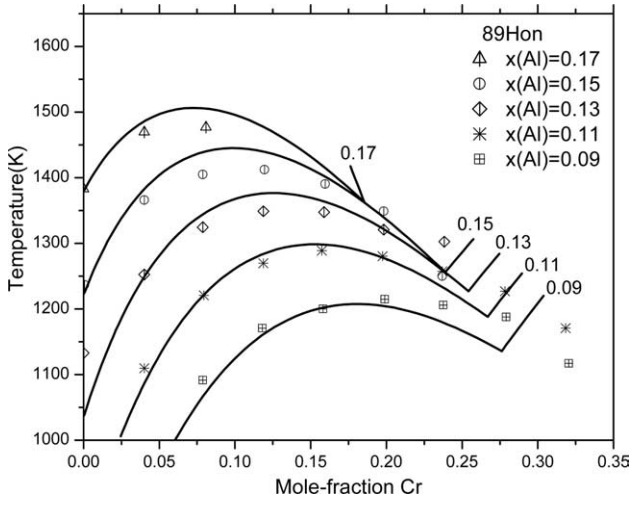

Fig. 7. Comparison of the CSA-calculated γ solvus of constant Al concentrations with the experimental data.

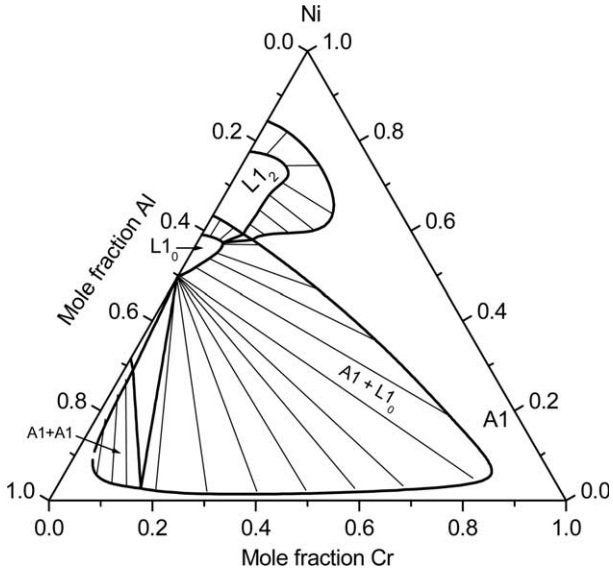

Fig. 8. CSA-calculated metastable fcc phase diagram at 1273 K.

temperatures and transforms to the ordered $L1_2$ and $L1_0$ structure as the temperature decreases. In view of the lack of stability of the A1 and $L1_2$ states in the Al-rich region, a miscibility gap occurs in the A1 phase. The calculated topology of equilibria involved the fcc-based phases is the same as that calculated from a "first principle" + CVM calculation [13,14]. The only difference is their calculated transformation temperatures are too high, i.e., they overestimate the stability of the ordered phases.

This good topological agreement of the CSA and CVM calculated fcc metastable phase diagram may be contrasted with the results obtained from previous descriptions using models based on the point approxi-

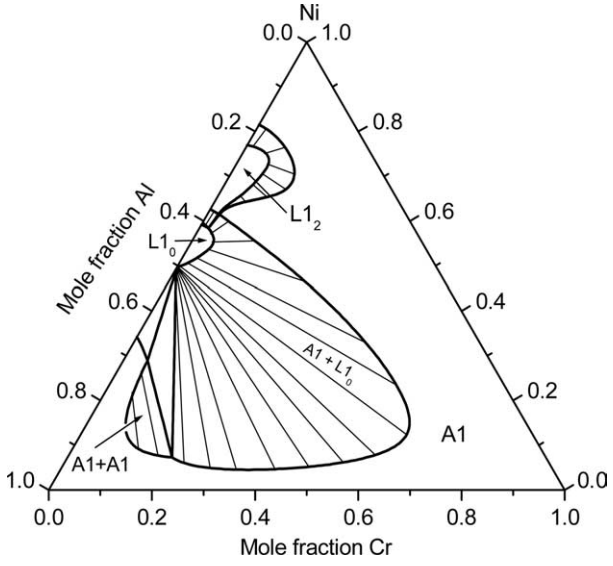

Fig. 9. CSA-calculated metastable fcc phase diagram at 1473 K.

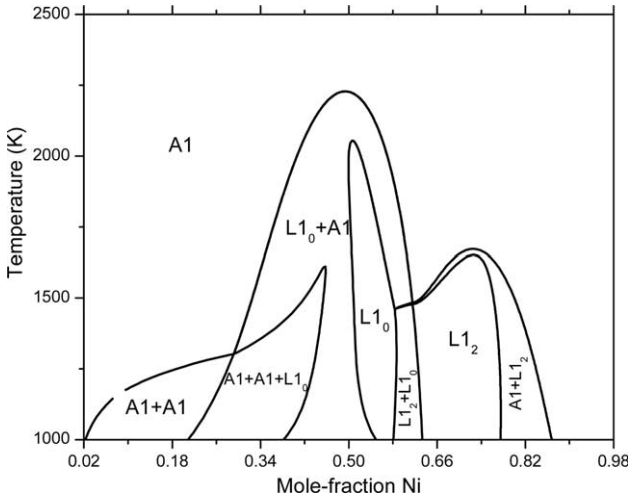

Fig. 10. CSA-calculated metastable fcc phase diagram of constant Cr = 0.02.

mation. The latter give problems with the topology of the fcc metastable phase diagram even when the stable phase diagrams obtained from these descriptions are in quite good agreement with the experimental data. Since the point approximation descriptions are known to give problems with the topology of fcc metastable binary phase diagrams [12], it can hardly be expected that they will give good descriptions of the metastable diagrams for ternary systems. These calculated metastable phase diagrams are important since they provide a better description of the non-equilibrium processes and microstructures in the Ni–Al–Cr system.

The CSA-calculated metastable fcc isothermal sections at 1273 and 1473 K are shown in Figs. 8 and 9, respectively. From Fig. 8, it can be seen that the γ(A1) is in equilibrium with the $\gamma'(L1_2)$, which corresponds with the stable phase diagram at 1273 K, while a misci-

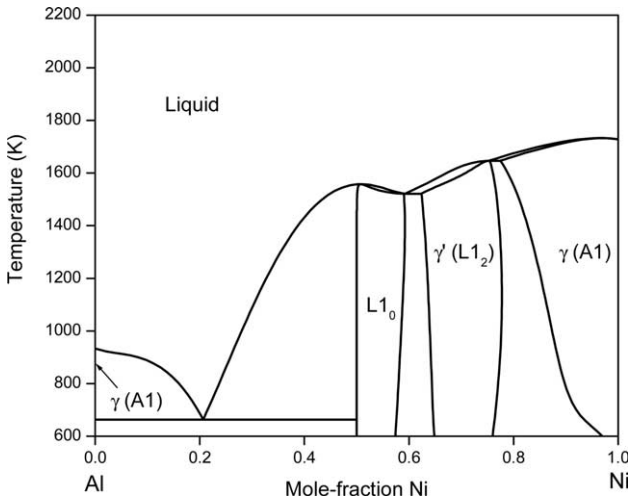

Fig. 11. CSA-calculated metastable Liquid + fcc phase diagram for Ni–Al binary system.

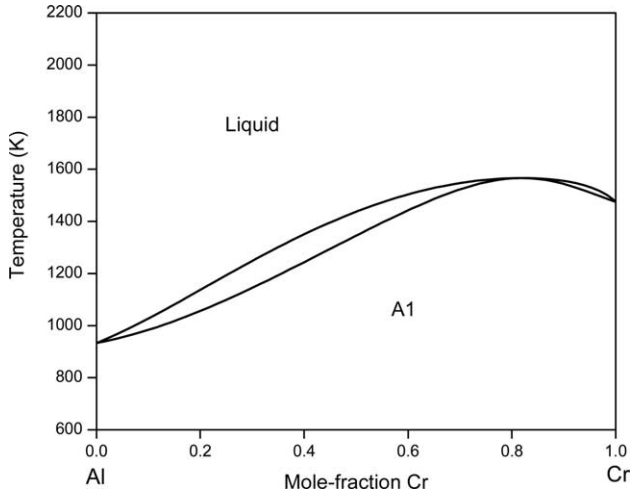

Fig. 12. CSA-calculated metastable Liquid + fcc phase diagram for Al–Cr binary system.

bility gap is found in the Al-rich corner. The ordered $L1_0$ extends from Ni–Al binary in the middle range compositions. Fig. 9 shows a similar topology but the $L1_2$ and $L1_0$ phase regions become smaller as the temperature increases, and when the temperature increases towards the critical point, the only existing phase would be the disordered A1 phase. It seems to be reasonable that the ordered $L1_2$ and $L1_0$ phases tend to form at low temperatures, while the disordered A1 phase is more stable at higher temperatures. In confirmation of this, a fcc metastable temperature-composition phase diagram was calculated by keeping the concentration of Cr at $x_{Cr} = 0.02$ as shown in Fig. 10. Topologically, it is similar to the metastable fcc phase diagram of Ni–Al binary and shows reasonable ordering/disordering behavior and phase relationships.

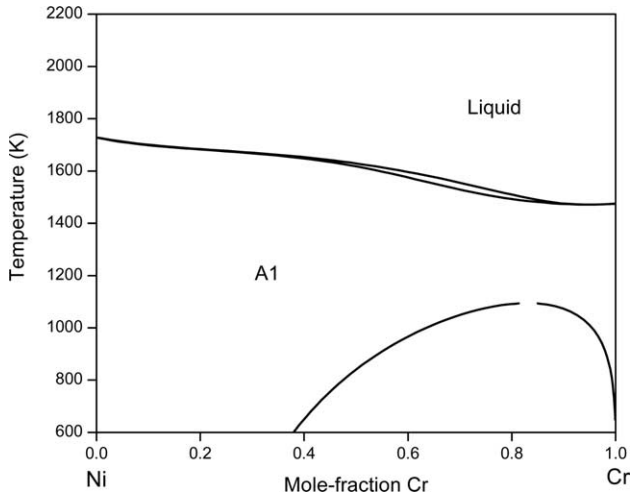

Fig. 13. CSA-calculated metastable Liquid + fcc phase diagram for Ni–Cr binary system.

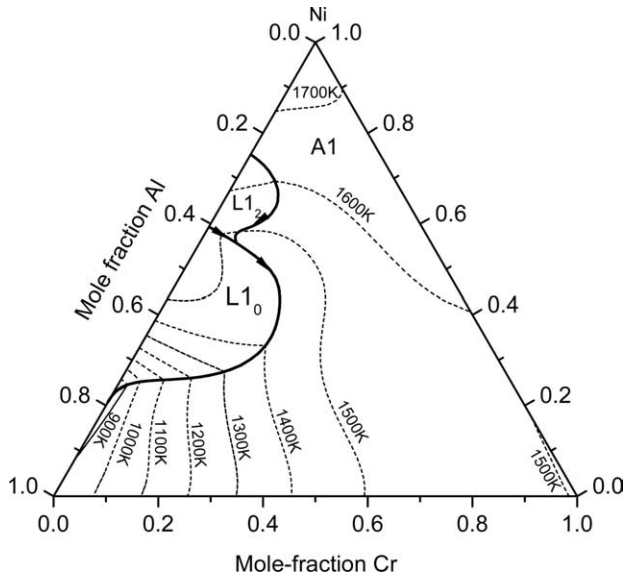

Fig. 14. The Ni–Al–Cr liquidus projection calculated by considering Liquid + fcc phases.

In addition, some metastable Liquid + fcc phase diagrams have been calculated using the current description. Those diagrams for the three binaries Ni–Al, Al–Cr and Ni–Cr are shown in Figs. 11–13, respectively. Fig. 14 shows the liquidus projection calculated by considering only the L and fcc phases, and there is an invariant equilibrium of class II at about 7 at.%Cr and 1490 K, Liquid + $L1_2$ = $L1_0$ + A1. This can be conformed by two isothermal sections calculated at 1273 and 1473 K, shown in Figs. 15 and 16, respectively. The two three-phase equilibria, L + $L1_0$ + A1 and $L1_2$ + $L1_0$ + A1 can be found in both figures, and the

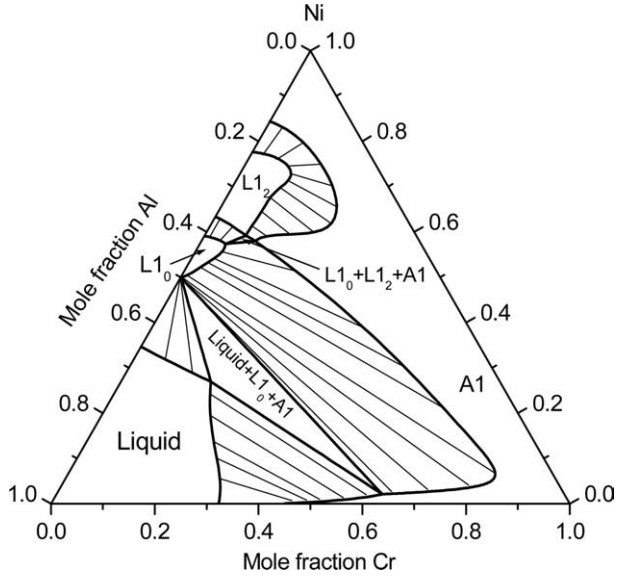

Fig. 15. CSA-calculated metastable Liquid + fcc phase diagram at 1273 K.

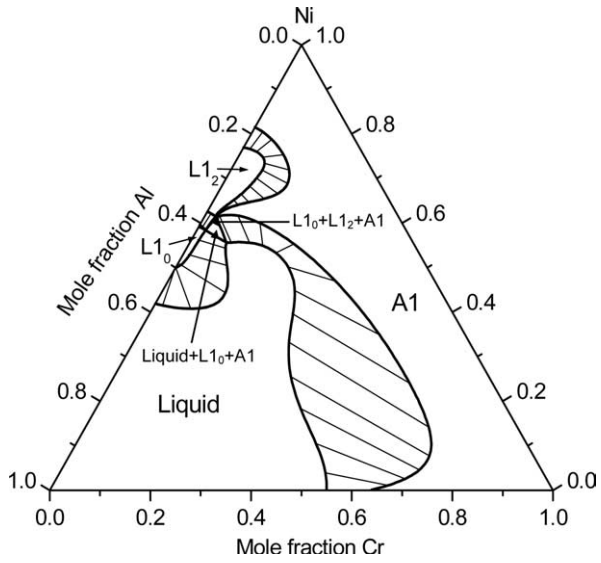

Fig. 16. CSA-calculated metastable Liquid + fcc phase diagram at 1473 K.

two three-phase regions become smaller and smaller as the temperature increases. When the temperature approaches to 1490 K, the invariant equilibrium L + $L1_2$ = $L1_0$ + A1 forms, as indicated in Fig. 14.

Thin films of the intermetallic phase γ'-$L1_2$ in the Ni–Al–Cr system have potential applications as protective high-temperature oxidation resistant coatings on gas turbine and aerospace components. The methods to obtain such a thin film varied from sputter deposition, laser ablation, evaporation and melt spinning. These methods are far away from being equilibrium processes due to the rapid quenching rate and lead to the formation of metastable phases such as the disordered fcc phase or the amorphous phase in the deposited thin film. The phase evolution of the metastable phases from disordered fcc or L to ordered state (γ'-$L1_2$) is critical for the material design and processing control. By using the CSA to describe the fcc phases, the calculated metastable phase diagrams involving the γ-A1, γ'-$L1_2$, $L1_0$ and/or liquid phase display correct topologies and could be especially useful for understanding phase transformation under conditions far away from equilibrium.

5. Conclusions

The phenomenological calculation of multi-component phase diagrams is an important tool for alloy development and process optimization. The use of the point approximation in the traditional CALPHAD approach produces errors in the phase diagram topology, particularly for fcc-based systems, due to the neglect of SRO in the calculation of the configurational contribution to the free energy. The CVM considers SRO and is able to give the correct topology for fcc-based systems. However, it is not a practical solution for multi-component systems since it introduces severe computational problems due to the large number of independent variables associated with the different cluster types in its free energy functional. This is to be contrasted with the CSA where the independent variables are greatly reduced to the sublattice site occupation probabilities by the adoption of a two-term configurational entropy expression. The CSA offers accuracy comparable to that achieved using the CVM without significant computational overhead, and may be used in multi-component systems.

The present study has focused on using the CSA to give a phenomenological description of the fcc phases in the real Ni–Al–Cr ternary system. The calculated stable phase diagrams from the current study show good agreement with the experimental data and the calculated metastable diagrams involving the fcc phases and Liquid plus fcc phases are topologically correct. They are believed to offer a better understanding of microstructures relevant to design the coating and thin film structure of the Ni–Al–Cr system through non-equilibrium processes such as sputtering and rapid quenching.

Acknowledgment

Financial support from the AFOSR Grant No. F49620-03-1-0083 is gratefully acknowledged.

References

[1] Huang W, Chang YA. Intermetallics 1998;6:487;
Huang W, Chang YA. Corrigendum: Intermetallics 1999;7:625.
[2] Dupin N. Contribution to the thermodynamic evalution of multicomponents Ni-base alloys. PhD thesis, Institute National Ploytechnique de Grenoble, France; 1995.
[3] Sundman B, Agren J. J Phys Chem Solid 1981;42:297.
[4] Dupin N, Ansara I, Sundman B. Calphad 2001;25:279.
[5] Shockley W. J Chem Phys 1938;6:130.
[6] De Fontaine D. Configurational thermodynamics of solid solutions. Solid state physics, vol. 34. New York (NY): Academic Press; 1979. p. 73.
[7] De Fontaine D. Cluster approach to order–disorder transformations in alloys. In: Ehrenreich H, Turnbull D, editors. Solid state physics, vol. 47. New York (NY): Academic Press; 1994. p. 33–176.
[8] Kikuchi R. Phys Rev 1951;81:988.
[9] Oates WA, Wenzl H. Scripta Mater 1996;35:623.
[10] Oates WA, Zhang F, Chen S, Chang YA. Phys Rev B 1999;59:11221.
[11] Cao W, Chang YA, Zhu J, Chen S, Oates WA. Acta Mater 2005;53:331.
[12] Zhang F, Chang YA, Du Y, Chen S-L, Oates WA. Acta Mater 2003;51:207.
[13] Carlsson AE, Sanchez JM. Solid State Commun 1988;65:527.
[14] Pasturel A, Colinet C, Paxton AT, van Schilfgaarde M. J Phys Condens Matter 1992;4:945.

[15] Fowler RH. In: Statistical mechanics. Cambridge: Cambridge University Press; 1938. p. 162.
[16] Yang CN. J Chem Phys 1945;13:66.
[17] Yang CN, Li Y. Chin J Phys 1947;7:59.
[18] Li Y. J Chem Phys 1949;17:447.
[19] Li Y. Phys Rev 1949;76:972.
[20] Ackerman H, Crusius S, Inden G. Acta Metall 1986;34:2311.
[21] Van Baal CM. Physica (Amsterdam) 1973;64:571.
[22] Ferreira LG, Mbaye AA, Zunger A. Phys Rev B 1988;37:10547.
[23] Zhang F, Chen S-L, Chang YA, Oates WA. Intermetallics 2001;9:1079.
[24] Zhang J, Oates WA, Zhang F, Chen S-L, Chou K-C, Chang YA. Intermetallics 2001;9:5.
[25] PANDAT™ Software for Multicomponent Phase Diagram Calculation is available from Computherm LLC, 437 S. Yellowstone Drive, Suite 217, Madison, WI 53719, USA.
[26] Taylor A, Floyd RW. J Inst Met 1952;8:1451.
[27] Ochiai S, Oya Y, Suzuki T. Bull P M E (T I T) 1983;52:1.
[28] Qiao Q. M.S. thesis, Interdiffusion microstructure in diffusion couples, University of Connecticut, 1998.
[29] Yeung CW, Hopfe WD, Morral JE, Romig Jr AD. In: Morral JE, Schiffman RS, Merchant SM, editors. Experimental methods of phase diagram determination. Warrendale, PA: The Minerals, Metals and Materials Society; 1994. p. 39–44.
[30] Hong YM, Nakayima H, Mishima Y, Suzuki T. ISIJ Int 1989;29:78.